

Nanoscale

Accepted Manuscript



This is an *Accepted Manuscript*, which has been through the Royal Society of Chemistry peer review process and has been accepted for publication.

Accepted Manuscripts are published online shortly after acceptance, before technical editing, formatting and proof reading. Using this free service, authors can make their results available to the community, in citable form, before we publish the edited article. We will replace this *Accepted Manuscript* with the edited and formatted *Advance Article* as soon as it is available.

You can find more information about *Accepted Manuscripts* in the [Information for Authors](#).

Please note that technical editing may introduce minor changes to the text and/or graphics, which may alter content. The journal's standard [Terms & Conditions](#) and the [Ethical guidelines](#) still apply. In no event shall the Royal Society of Chemistry be held responsible for any errors or omissions in this *Accepted Manuscript* or any consequences arising from the use of any information it contains.

Stable ligand-free stellated polyhedral gold nanoparticles for sensitive plasmonic detection

Rachel Keunen, Danielle Macoretta, Nicole Cathcart and Vladimir Kitaev

Department of Chemistry and Biochemistry, Wilfrid Laurier University,

75 University Avenue W, Waterloo, Ontario, Canada N2L 3C5

Abstract:

Ligand-free stellated gold nanoparticles (AuStNPs) with well-defined octahedral (O_h) and icosahedral (I_h) core symmetries were prepared using hydrogen peroxide as a reducing agent. Only three reagents: gold precursor ($HAuCl_4$), H_2O_2 and NaOH were required to form colloiddally and chemically stable AuStNPs with a zeta-potential between -55 and -40 mV indicative of excellent charge stabilization. The size and degree of stellation of AuStNPs can be controlled by several synthetic parameters so that the localized surface plasmon resonance (LSPR) can be varied from ca. 850 nm in near-infrared (NIR) to ca. 530 nm. In particular, AuStNP size and LSPR tuning can be conveniently accomplished by iodide variation. The size distribution of AuStNPs was improved by nucleation with ascorbic acid, and the AuStNP size and degree of branching could be readily modified using arginine. AuStNPs are advantageous for SPR sensing, as it was demonstrated in the sensitive detection of not only thiols, such as ampicillin, but also iodide with the detection limit of 3.2 pM (0.4 ng/L). The reported ligand-free stable AuStNPs

* E-mail: vkitaev@wlu.ca

thus should be very useful for biodiagnostics based on SPR sensing and potentially for SERS and hyperthermia therapy.

Introduction

Metal nanoparticles (MNPs) have established themselves on research frontiers owing to their unique nanoscale properties,^{1,2} such as localized surface plasmon resonance (LSPR)^{3,4} and to their wide range of promising applications, e.g. in optics,⁵ catalysis,⁶ sensors⁷ and surface-enhanced Raman spectroscopy.⁸

Among MNPs, gold nanoparticles, AuNPs, feature superior chemical stability.⁹ AuNPs can withstand aggressive chemical environments in comparison with the more morphologically diverse, but less stable silver nanoparticles, AgNPs.^{2,10} The inertness and biocompatibility of gold makes AuNPs advantageous for medical applications.¹¹ Common procedures of AuNP synthesis, e.g. reduction with citrate,¹² yield spherical AuNPs with LSPR maxima typically ranging from ca. 520 to 550 nm.¹³ For many applications, LSPR in NIR is desirable and advantageous due to the so-called “biological windows” of relative optical transparency at 600–950 nm and 1000–1350 nm.¹⁴ Achieving NIR LSPR is not practical with spherical AuNPs due to large sizes required,¹³ and interfering emergence of quadrupolar resonances with the resulting broadening of LSPR peaks.¹⁵

One of the effective approaches to prepare gold nanostructures with LSPR in the NIR range involves preparation of gold shells templated over AgNPs.^{16,17} This powerful strategy enables preparation of a variety of gold nanostructures with diverse morphologies and functional

properties. Limitations of gold templating are in the availability and quality of silver NP templates;¹⁸ as well as the need to account for the residual silver in the system.

Another approach to the synthesis of AuNPs with NIR LSPR is the formation of branched, also referred to as “star” or “stellated”, nanoparticles.^{19,20,21} Long branches and concavities are effective to shift the LSPR into the NIR, with the degree of concavity and the sharpness of branches/extremities enabling convenient LSPR tuning. Concave shapes are also advantageous for SERS due to strong field enhancement in the cavities.^{22,23,24} Plasmonic²⁵ and biological²⁶ applications of stellated AuNPs are actively explored.

There have been several examples of star-shaped, stellated and dendritic AuNPs reported in the literature in the last decade, the majority of which utilize cationic surfactants, such as cetyltrimethylammonium bromide (CTAB).^{27,28} Sau and Murphy first reported a synthesis using AuNP seeds, CTAB, ascorbic acid and NaBH₄ which resulted in a yield of ~50% and a NP size of 66 nm.²⁷ Nehl *et al.* synthesized dendritic AuNPs using a similar approach that started with 10 nm gold seed particles.¹⁹ In a synthesis reported by Langille *et al.* CTACl or CTAB, 7 nm AuNP seeds, ascorbic acid and NaBr were employed to produce dendritic AuNPs.²⁸ Yamamoto *et al.* reported a synthesis of star-shaped gold nanoplatelets using HAuCl₄, ascorbic acid, and poly(*N*-vinylpyrrolidone) (PVP) at a pH of 2.3 that resulted in 7% dendritic AuNPs.²⁹ Similarly Huang, Meng and Qi reported a synthesis of polydisperse planar dendritic AuNPs using HAuCl₄, DTAB, β-CD, and ascorbic acid in solution for 27 h at 27 °C.³⁰ The strategies of the seeded growth were recently nicely explored by Skrabalak’s group to prepare diverse symmetric dendritic stellated nanostructures of gold, as well as several bimetallic NPs.^{31,32,33}

For the majority of biological applications, CTAB needs to be removed from AuNPs which can be challenging, especially given the large excess of CTAB used for synthesis.²⁷ CTAB toxicity is

one of the contributors to the controversy on AuNP toxicity.³⁴ Thus, AuNPs with biologically-friendly ligands or so-called “ligand-free” AuNPs are desirable.

Star-shaped gold nanoparticles have been also prepared using citrate as a stabilizing ligand in a seeded regrowth method in the presence of silver ions and ascorbic acid as a reducing agent.³⁵ These stellated nanoparticles featured variable LSPR from visible into NIR and were demonstrated useful for *in vivo* imaging.

Hydrogen peroxide was actively explored recently as, perhaps, a counterintuitive but effective reducing agent for the formation of AuNPs.^{36,37,38} One of the inspiring works in this field that motivated further research is the formation of AuNPs with hydrogen peroxide in an ELISA-based sensing mechanism reported by de la Rica and Stevens.³⁶ Several works expanded upon this report by using hydrogen peroxide in AuNP synthesis for applications in sensing.^{37,38,39} This research was largely focused on sensing applications, thus size and shape control has not been fully explored. At the same time, narrow AuNP size distribution and shape selection are highly advantageous for sensing applications.^{40,41}

Herein we report on the synthesis of highly symmetric stellated gold nanoparticles (AuStNPs) using hydrogen peroxide as a reducing agent. This developed approach establishes convenient ligand-free preparation where the nanoparticle size and degree of stellation can be regulated by several parameters, such as reaction conditions, use of seed particles and moderate etching with iodide. With the control of the AuStNP size and degree of stellation, the LSPR can be maneuvered from 530 to 850 nm. Iodide sensing through LSPR changes of ligand-free AuStNPs with the detection limit of 3.2 pM has been demonstrated. The absence of ligands and consequent ease of surface modification open venues for AuStNP applications in *in vivo* or *in vitro* biological assays and diagnostics.

Results and Discussion

General Details/Features. The schematic of the AuStNPs synthesis is summarized in Figure 1A,B). Working with different conditions of AuNP synthesis by reduction with hydrogen peroxide, it was discovered that the most effective reaction systems that can yield stable stellated AuNPs are strikingly simple. Only HAuCl_4 (a common gold precursor), H_2O_2 as a reducing agent, and a strong base (NaOH) for triggering the reduction reaction, as well as for AuStNP stabilization are required. Once the reaction is triggered, it proceeds very fast as the reducing agent is in huge excess ($>500:1$ molar ratio of H_2O_2 to Au). Consequently, the AuStNP growth is effectively diffusion-limited, and the resulting AuStNP size and degree of stellation are strongly dependent on stirring speed and triggering conditions of the reduction, such as pH. Representative optical photographs of AuStNPs are shown in Figures 1C and S1; electron microscopy images are given in Figure 2.

In the absence of strongly binding capping ligands, the typical size of synthesized AuStNPs is relatively large in the range from ca. 80 to 200 nm (Figs. 2, S3). There are two predominant shapes of the stellated morphologies of AuStNPs; one with O_h core symmetry that can be identified by its characteristic combination of 4-fold and 3-fold symmetry axes that are readily distinguishable in SEM images as crosses (Fig. 2A) or squares (Fig. 2B), and second with I_h core symmetry with its characteristic 5-fold projections (Figs. S3B, F). AuStNPs with well-defined D_{5h} core symmetry (decahedra, pentagonal bipyramids) were not observed. At the current stage of this work, we are not able to find appropriate conditions for shape-selective synthesis yielding a single type of the core symmetry. It can be noted that, AuStNPs with the octahedral symmetry are a predominant product for the optimal reaction conditions that reproducibly yield larger

particles (e.g. see Fig. 2A and Table S1). The dominance of octahedral defect-free AuStNP morphologies is reasonably expected for larger noble metal nanoparticles based on the stability of their seed nanoclusters^{42,43,44} Given the varying degree of branching and rough dendritic-like surface resulting from the diffusion limited growth, the identification of higher crystallographic planes of AuStNPs may not be instructive.

Triggering AuStNP synthesis with NaOH. Hydrogen peroxide is more commonly thought of and used as a strong oxidizing agent. However, since H₂O₂ red-ox potential as both an oxidizing and a reducing agent are strongly pH-dependent, hydrogen peroxide can serve as a reducing agent in basic conditions: $\text{H}_2\text{O}_2 + 2\text{OH}^- = 2\text{H}_2\text{O} + \text{O}_2 + 2\text{e}^-$

The standard potential for this reaction is ca. 0.6 V at pH = 14. So the reduction of Au³⁺ with its standard potential of +1.5 V is expected to occur favourably and indeed is readily observed in basic pH. At neutral pH, the gold reduction reaction is observed to be sluggish,⁴⁵ and larger aggregated particles are formed upon this slower reduction. In typical conditions of AuStNP synthesis, the concentration of the gold precursor, tetrachloroauric acid, is relatively low in a range of 0.1 to 1 mM, so that gold reduction requires stronger reducing conditions. Practically, the AuStNP formation triggered by NaOH was observed to be optimal in the range of pH from 10.5 to 11.8. Above pH of 11.8-12, the reduction becomes too fast for uniform mixing, also the concentration of NaOH becomes too high for convenient safe handling. Below pH of ca. 10.5, the reduction becomes sluggish and results in formation of less defined morphologies of AuNPs. At the same time, upon mixing of HAuCl₄ and H₂O₂, slow partial reduction of gold is observed (precipitating metallic gold within few days). Thus, after mixing tetrachloroauric acid and hydrogen peroxide, the immediate NaOH addition is the best reaction protocol to follow. Encouraged by the recently reported gold structures where pre-reduction of gold precursors

played a formative role in shape selection,⁴⁶ we have explored an approach where NaOH addition was delayed. No influence on shape selection was found for AuStNPs formed with delayed addition of NaOH, only a broader size distribution was observed; a likely reason for that is the absence of ligands directing the seed formation in the system. Overall, upon triggering reduction reaction with NaOH at an optimal pH of ca. 11.5 (see *Experimental in ESI* and Table S1) we were able to attain well-defined stellated morphologies with reproducibility in size and LSPR (Figs. 2,3 and S3).

Comparison of hydrogen peroxide role in the synthesis of AuNPs and AgNPs. Since hydrogen peroxide is commonly used for the preparation of silver nanoparticles, AgNPs, its different roles for AuNPs and AgNPs can be outlined briefly. For AgNPs, which are appreciably more reactive compared to AuNPs, hydrogen peroxide serves as an oxidant which brings a red-ox equilibrium and formation of platelets/prisms as a kinetically-favourable shape.^{47,48} Usage of hydrogen peroxide was first reported by Mirkin's group,⁴⁹ who previously used air as an oxidant in their seminal papers on preparation of silver nanoprisms.⁵⁰ Hydrogen peroxide is not able to etch gold nanoparticles. For AuNPs, such as current AuStNP synthesis, hydrogen peroxide serves as a reducing agent in basic or neutral pH.

Role of experimental parameters (stirring, reagent concentrations and order of reagent addition). Since the reduction of tetrachloroauric acid by hydrogen peroxide is effectively triggered by NaOH (or greatly enhanced from occurring within a few days to a few seconds), it would be reasonable to expect that for the uniform and homogenous reduction reaction, NaOH is optimally added last. This reagent addition order is different from typical nanoparticle preparations where a reducing agent is commonly added last. For this reason, we have compared different order of reagent additions (Fig. S4) The results show very strong effects of the reagent

order for this diffusion-limited reaction. For instance, adding peroxide last leads to very broad particle size distribution with its characteristic very broad featureless spectra (spectra 5 and 6 in Fig. S4). At the same time, NaOH added last yields good well-defined AuStNPs (spectra 3 and 4 in Fig. S4). When gold is added last, the influence of stirring rate was found to be very strong since the stirring is crucial to assure that uniform precursor reduction takes place. Experimentally, it is often quite challenging to attain uniform fast stirring rates with high reproducibility. Consequently, experimental protocols with NaOH added last have been adapted to prepare well-defined AuStNPs reproducibly.

In a diffusion-limited reaction, a relatively high concentration of gold at 0.5-0.8 mM was important for the well-developed stellation. AuStNPs prepared with lower amounts of gold are noticeably less stellated with the appearance of ill-defined rough polygons (Figs. 2C, S5A).

Overall, to prepare uniform AuStNPs reproducibly, high stirring rate of 700 rpm (using a common small magnetic stirring bar – see *Experimental in ESI*) was found to be optimal. The high stirring assures that reagents are distributed uniformly for a homogenous reaction of nanoparticle formation, especially nucleation in this diffusion-limited reaction.

Effect of iodide in AuStNP synthesis (convenient tuning of particle size and LSPR). We have started to explore iodine in AuNP synthesis to assist shape selection by dissolving less stable AuNPs. Working with hydrogen peroxide, we realized that iodine can be conveniently generated *in situ* by oxidation of iodide by hydrogen peroxide. Indeed, iodide addition had a pronounced effect on formation of AuStNPs. With increase in iodide concentration in the reaction system, AuStNPs become progressively less stellated and more compact, which is evident in an appreciable LSPR blue shift to ca. 530 nm (Fig. 3B). The pronounced effect of iodide is observed at concentrations as low as 4 nM (Fig. 3B). The strong iodide effect is similar to what

was discovered by Mirkin's group for the synthesis of gold nanorods.⁵¹ The plausible mechanism of the strong iodide effect is that iodine is capable of dissolving and thus effectively transferring gold from the high-energetic points, such as branches, to the lower energy areas of cavities. The transfer of gold would assist in reaching effective pathways to the most thermodynamically stable compact morphologies with LSPR at 530-550 nm. Overall, the addition of iodide allows LSPR variation from ca. 850 nm (in absence of iodide) to ca. 530 nm of small compact particles (Figure 3).

It is possible to control the size and degree of stellation of AuStNPs using factors such as pH and hydrogen peroxide concentration, as described in previous sections. Yet, the addition of KI offers an approach for the controlled variation of size and LSPR in AuStNPs that is very straightforward and simple to implement experimentally. The strong effect of iodide on AuStNP synthesis can be also used for post modification of AuStNPs and sensing experiments (see Section on Sensing below).

Seeded growth and nucleation with ascorbic acid. In order to improve AuStNP size dispersity and to influence shape selection in the system, we have performed several experiments with the seeded growth. First, the regrowth of AuStNPs was tested to aim at larger particles and to potentially focus the size distribution. In these experiments, previously formed AuStNPs were introduced as seeds with the amount of $\frac{1}{4}$ relative to the total gold amount, which remained the same as in one-stage AuStNP synthesis (see *Experimental in ESI*). The main outcome of these experiments was AuStNPs with a decreased extent of stellation and only moderate increase in AuStNP size (Figs. S5C,D). First, the AuStNP seeds did not grow exclusively, secondary nucleation was apparent; and the second, most of the new gold deposited in the low-energy

cavity locations on the seed nanoparticles. Thus, it can be concluded that the diffusion-limited growth of AuStNPs is not compatible with seeded regrowth.

Another seeding strategy investigated was to introduce a small amount of a stronger reducing agent prior to or together with the triggering reaction by NaOH. We selected ascorbic acid, which is a common reducing agent for gold and silver⁵² and which is also known to generate radicals with peroxide rapidly and thus further strongly influence AuStNP nucleation. In a typical procedure, NaOH and ascorbic acid were premixed for the addition as a final component in the synthesis to trigger the reduction reaction (Fig. S6). Indeed, addition of small amounts of ascorbic acid (ca. 1:5 molar to gold) was a successful approach. With ascorbic acid, the resulting AuStNP size distribution was improved and further control over AuStNP size could be exercised (Table S1, Figs. S6C,D). At the same time, larger amount of ascorbic acid resulted in formation of smaller shapeless particles (Fig. S6B). As a result, it can be concluded that the strategy based on addition of small amount of a stronger reducing agent to trigger selective seeding is a powerful approach that works well for AuStNPs. Using ascorbic acid enabled to produce AuStNPs with shaper LSPR peaks ranging from ca. 500 to 680 nm.

Effect of ligands on AuStNP morphology: example of arginine. In exploring experimental parameters of AuStNP synthesis we have tested the effect of biological molecules that can potentially affect nucleation by serving as capping ligands for AuNPs. Given the high negative zeta potential of AuStNPs, it was instructive to explore arginine since it serves as a good capping agent for negatively charged surfaces.⁵³ Arginine is also known to complex silver and gold,⁵⁴ and the use of another basic amino acid, lysine, was reported for the preparation of gold star nanoparticles.⁵⁵ Arginine, indeed, was effective in nucleating and capping the surface of AuNPs. The resulting AuNPs became much smaller, typically with the diameter of around 30 nm (Fig.

S5B) while at the same time featuring LSPR maxima at ca. 550-620 nm (Table S1) due to rough agglomerated structure of AuNPs (Fig. S5B). At the same time, the polyhedral symmetry was largely lost.

Chemical and colloidal stability of AuStNPs. Since AuStNPs were prepared in absence of capping ligands, their stability were carefully evaluated. Surprisingly, as prepared AuStNPs were perfectly colloidally stable more than 2 years since the preparation of the first samples in our laboratory. Colloidal dispersions of AuStNPs sediment within few days. Upon gentle shaking the sedimented dispersions can be restored to their original state with the same average particle size by Zetasizer and UV-vis spectra. For AuStNPs prepared without organic additives (such as ascorbic acid), only a minor blue LSPR shift of 5-10 nm was observed for several days to several months after preparation, likely due to a minor loss of sharp features. AuStNP samples seeded with ascorbic acid retained colloidal stability but experienced a noticeable blue LSPR shift upon decrease in stellation and conversion to more compact particles. AuStNPs also featured a surprisingly large negative zeta potential (as high as -55 – -60 mV, see Figure S7), which is indicative of excellent charge stabilization. Since there are no capping ligands in the system and the oxidation products of hydrogen peroxide are oxygen and water – the most likely scenario is that OH⁻ ions adsorb appreciably at AuStNP surface in absence of other ligands and ions except chloride. Changes in zeta potential of AuStNPs upon titration with HCl is shown in Figure S8 and Table S2. It can be seen that zeta-potential of AuStNPs decreases steadily upon HCl addition. AuStNPs retain slightly negative potential of ca. -10 mV upon NaOH neutralization (Fig. S8 and Table S2) and aggregate slowly within a few minutes. Thus, the charge stabilization is a primary stabilization mode of AuStNPs; and chloride adsorption can be excluded from significantly affecting charge stabilization. An additional factor that is likely to further enhance

AuStNP stability and resistance to aggregation originates from the geometry of stellated morphologies: the contact area between particles upon their physical contact is minimized by non-commensurate protrusions. Alternatively, higher OH^- adsorption can be attributed to higher-energy high-index crystallographic facets in stellated nanostructures.⁵⁶

The ligand-free surface of AuStNPs adsorbs OH^- in the absence of other strongly adsorbing ions and ligands. Addition of stronger binding CTAB causes recharging of zeta potential to positive values of ca. 22 mV (Fig. S9). AuStNPs nicely retain colloidal stability with CTAB stabilization, as indicated by minimal changes in UV-vis spectra. Citrate also likely adsorbs onto the AuStNP surface. AuStNPs remain stable and negatively charged upon citrate addition. For higher citrate to gold ratios (8 to 20 molar) that are close to commonly used for stabilization of metal nanoparticles, the zeta-potential values of citrate-modified AuStNPs in the range of -50 mV indicate excellent stability (Fig. S9). Citrate adsorption can be further corroborated by relative stability of AuStNPs upon titration with citric acid. At citric acid to OH^- molar ratio of 2, AuStNPs still retained negative zeta potential of ca. -15 mV (Fig. S9), while upon titration with hydrochloric acid, zeta-potential became positive (Fig. S8).

The improved chemical stability of larger AuStNPs with correspondingly larger stellation was apparent in the case of exposure to arginine. There smaller AuStNPs aggregated appreciably at 0.01 M arginine and aggregated completely and irreversibly at 0.1 M (Fig. S10B curves 1-3), while larger AuStNPs were perfectly stable in 0.1 M arginine (Fig. S10B curves 4-5). Thiols are known to cause etching and degradation of noble metal particles due to the strong affinity of thiols to silver and gold. In this respect, AuStNPs were remarkably stable in 0.1 M cysteine (Fig. S10C) and 0.01 M ampicillin (Fig. S10D). Excellent colloidal, chemical and LSPR stability of

AuStNP in these various environments makes them good candidate nanoparticles for specific SPR sensing.

At the same time, AuStNPs were highly sensitive to iodide ions, especially larger particles. Figure S10A documents exposure of larger AuStNPs to 10^{-5} M iodide solution with the large LSPR shift of ca. 50 nm. At the same time, smaller AuStNPs were less sensitive to iodide, since being less stellated they experience a comparatively smaller loss of stellation. Transformation of stellated NPs to more stable compact particles is the main mode of iodide action on AuStNPs similar to the iodide effect in AuStNP synthesis.

Prototype sensing with AuStNPs

We have further explored iodide effect in prototype SPR sensing. Ligand-free AuStNP are very sensitive to the adsorption of iodide. The AuStNPs samples that were used for testing included those prepared with ascorbic acid and corresponding to the data of Figure 3A1 described in Table S1, as well as ligand-free AuStNPs similar to those described for Figure 2A&D. Addition of 10^{-10} M iodide to AuStNPs causes an appreciable large LSPR shift of 0.92 nm (Fig. 4A) relative to the signal background noise. With the LSPR signal noise of under 0.02 nm or 20 pm peak-to-peak (Fig. 4B), the detection limit at $S/N=1.5$ can be estimated as 3.2×10^{-12} M or 0.4 ng/L. Realistically, the detection limits are affected by the cell disturbance upon iodide addition and mixing. The SPR signal fluctuations associated with these disturbances are in the worst extremes below 0.2 nm, so the iodide detection limit is well above 3×10^{-11} M.

Bromide physisorption also causes SPR response of AuStNPs with at least 6 times less sensitivity from preliminary experiments. In contrast, the SPR response of AuStNPs to citrate can be detected only at 10^{-6} M. The reasons for the strong SPR sensitivity of AuStNP to iodide

and bromide are the absence of ligands on the surface and the higher surface area of stellated structures that likely significantly enhances the SPR response.

Upon exposure of AuStNPs to larger iodide concentrations higher than ca. 10^{-6} M, LSPR undergoes decrease due to the loss of stellation, as shown in Fig. 4C. The LSPR decrease due to the morphology change is small (under 1 nm) at 10^{-6} M, while at higher iodide concentration of 10^{-5} M LSPR maxima of AuStNP sample tested decreased more than 15 nm from 565 nm to under 550 nm. These morphological changes involving stellation take place relatively slow for ca. 5000 seconds compared with faster physisorption changes occurring for under 100 seconds at much lower iodide concentrations (Fig. 4A). Thiols, such as cysteine, glutathione and ampicillin also readily adsorbs onto a ligand-free surface of AuStNPs. Figure 4D shows LSPR response upon addition of two aliquots of ampicillin: 10^{-10} M and 10^{-9} M, respectively. Clearly, 10^{-10} M ampicillin can be readily sensed and the detection limit, estimated relative to fluctuations of the SPR signal background, is below 10^{-11} M. At the same, there is a saturation of the response likely due to ligand monolayer formation that results in subsequent weaker sensitivity to higher concentrations of adsorbing species. Larger LSPR shift outlines promising venue of exploring morphological changes for SPR sensing that can potentially offers higher sensitivity.

Conclusion

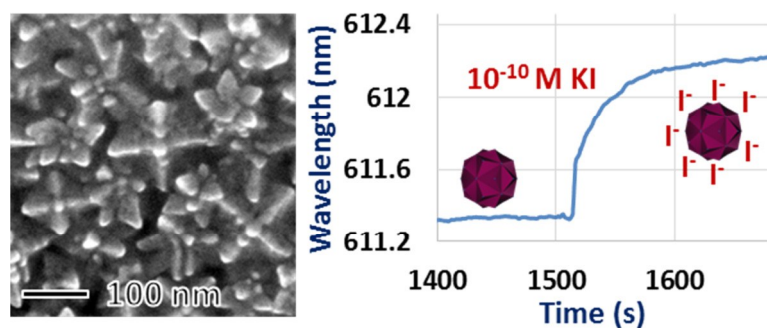
We have developed and described a set of convenient experimental protocols to produce ligand-free chemically stable stellated gold nanoparticles with SPR tunable from visible to NIR. The reported AuStNPs were shown to promising for the sensing applications based on their ligand-free surface sensitive to physisorption. Future work will explore applications of AuStNPs as a

SPR substrate and in surface-enhanced Raman spectroscopy, as well as gold-silver composites for enhanced plasmonic sensing.

Acknowledgements

The authors would like to thank NSERC (Discovery grant, graduate and UG scholarships), ACS PRF and Wilfrid Laurier University for funding. Centre for Nanostructure Imaging, University of Toronto, is acknowledged for access to imaging facilities, and Ilya Gourevich and Neil Coombs for their invaluable support with the electron microscopy.

TOC image



Stable stellated ligand-free gold nanoparticles were synthesized and demonstrated to be advantageous for sensitive LSPR detection

Figures.

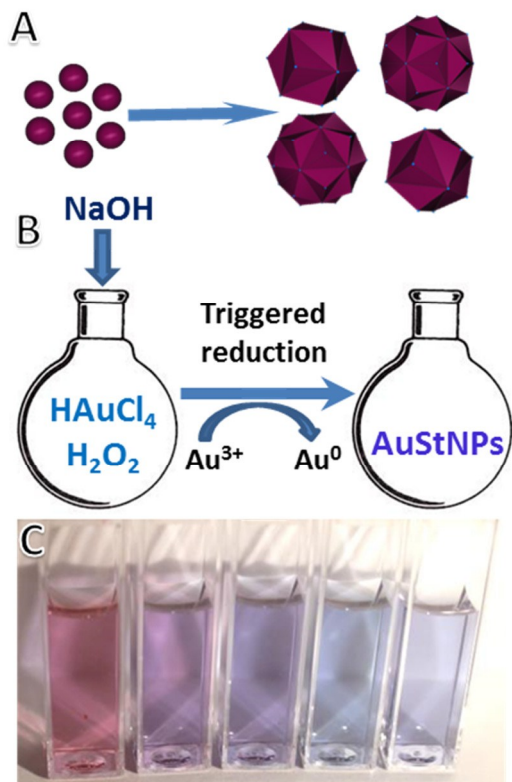


Figure 1. Schematics illustrating preparation of AuStNPs: **A)** morphological development of AuStNPs; **B)** the order of reagent addition and reaction progression. **C)** Optical photographs of AuStNP samples diluted 5 times after preparation.

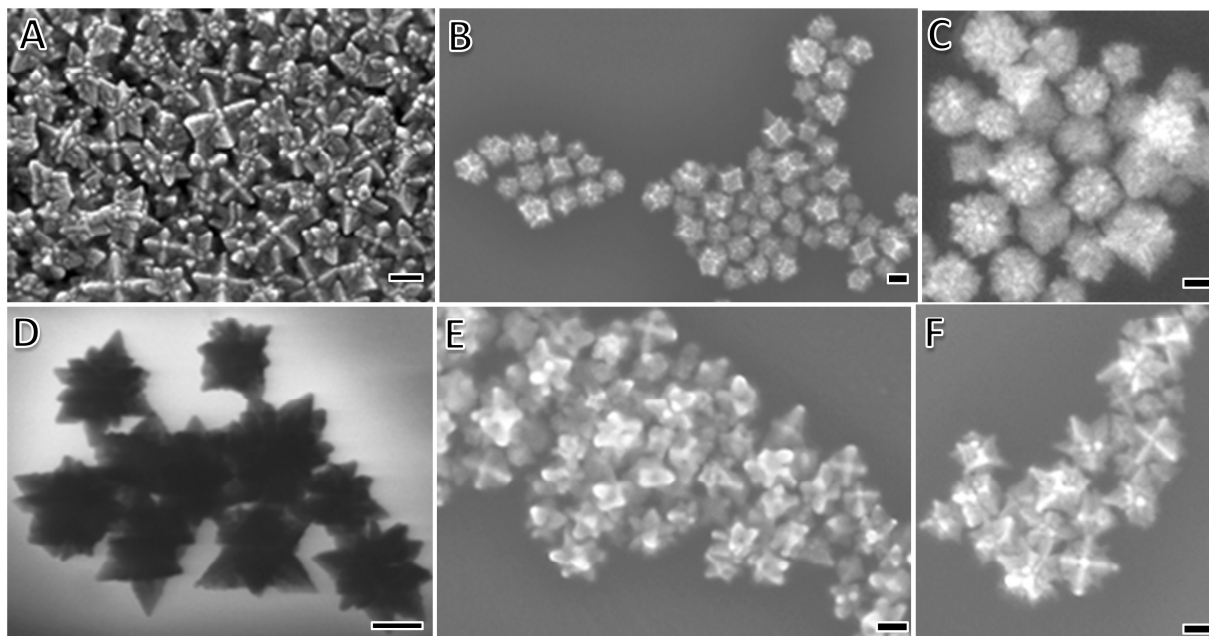


Figure 2. Representative electron microscopy images of AuStNPs. **D)** is a TEM image, the rest are SEM images. All scale bars are 100 nm. **A)** and **D)** – optimal conditions; **B)** higher gold concentration; **C)** lower gold concentration; **E)** lower hydrogen peroxide and higher NaOH concentrations; **F)** higher NaOH concentration. For detailed description of samples - see **Table S1**.

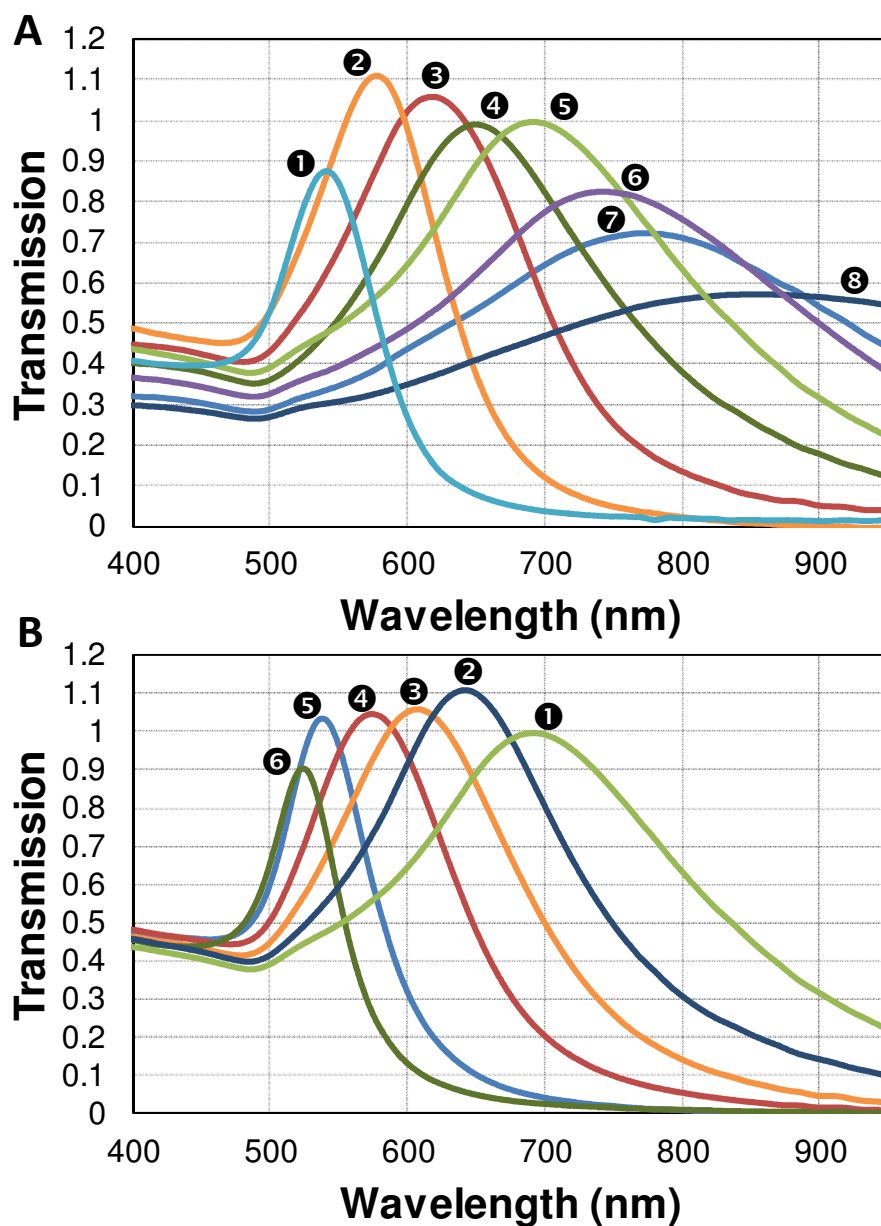


Figure 3. UV-vis spectra of AuStNP samples prepared **A)** without and **B)** with iodide to control the plasmon resonance from 525 nm to 850 nm. Synthetic parameters for **A)** are described in Table S1; total concentrations for samples in **B)** are as follows: 0.48 mM HAuCl_4 , 133 mM H_2O_2 , and 6.7 mM NaOH with varying KI: **1** 0 μM ; **2** 3.8×10^{-3} μM ; **3** 5.9×10^{-2} μM ; **4** 0.95 μM ; **5** 1.9 μM ; and **6** 6.89 μM . KI was added prior to peroxide and sodium hydroxide for these samples.

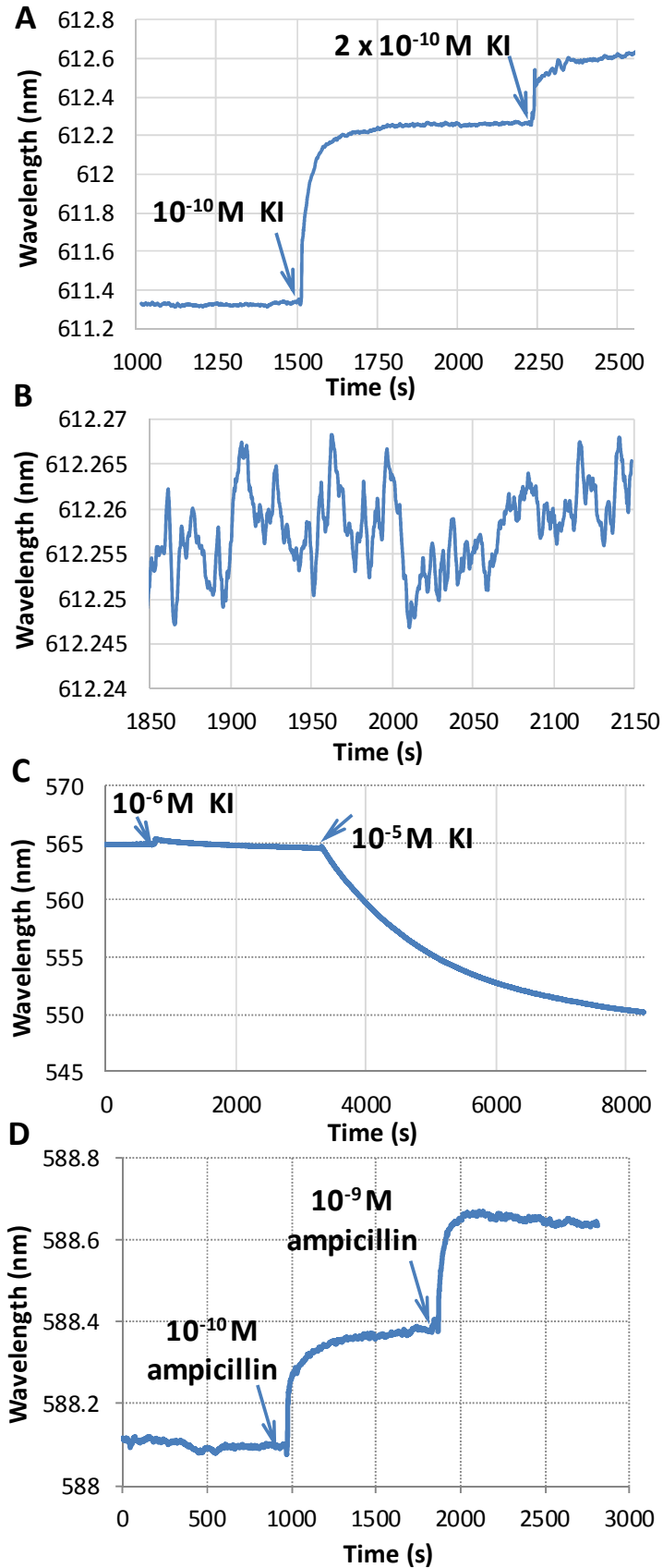


Figure 4. Surface plasmon resonance, SPR, sensing experiments showing the changes of LSPR maxima upon AuStNP exposure to iodide ions: **A)** SPR response to lower iodide concentrations – two additions of 10^{-10} M iodide indicated by the arrows with the LSPR increase upon iodide physisorption onto AuStNPs. **B)** SPR signal noise of under 0.02 nm (peak to peak); **C)** LSPR decrease upon exposure to higher iodide concentration of 10^{-5} M, with the first 10^{-6} M iodide addition shown for comparison (addition of iodide indicated by the arrows). **D)** SPR response to low ampicillin concentrations – two additions of 10^{-10} M and 10^{-9} M indicated by the arrows with the LSPR increase upon ampicillin physisorption onto AuStNPs.

References

- ¹ T. K. Sau, A. L. Rogach, F. Jäckel, T. A. Klar and J. Feldmann, Properties and applications of colloidal nonspherical noble metal nanoparticles. *Adv. Mater.*, 2010, **22**, 1805–1825.
- ² Y. Xiong and X. Lu, eds. *Metallic Nanostructures. From Controlled Synthesis to Applications*. Springer, 2015, pp. 1–49.
- ³ S. Eustis and M. A. El-Sayed, Why gold nanoparticles are more precious than pretty gold: noble metal surface plasmon resonance and its enhancement of the radiative and nonradiative properties of nanocrystals of different shapes. *Chem. Soc. Rev.*, 2006, **35**, 209–217.
- ⁴ G. Baffou and R. Quidant, Nanoplasmonics for chemistry. *Chem. Soc. Rev.* 2014, **43**, 3898–3907.
- ⁵ Q. Gan, F. J. Bartoli and Z. H. Kafafi, Plasmonic-enhanced organic photovoltaics: breaking the 10% efficiency barrier. *Adv. Mater.*, 2013, **25**, 2385–2396.
- ⁶ S. Linic, U. Aslam, C. Boerigter, and M. Morabito, Photochemical transformations on plasmonic metal nanoparticles. *Nature Mater.*, 2015, **14**, 567–576.
- ⁷ X. Yang, M. Yang, B. Pang, M. Vara and Y. Xia, Gold Nanomaterials at Work in Biomedicine. *Chem. Rev.*, 2015, **115**, 10410–10488.
- ⁸ L. A. Lane, X. Qian and S. Nie, SERS Nanoparticles in Medicine: From Label-Free Detection to Spectroscopic Tagging. *Chem. Rev.*, 2015, **115**, 10489–10529.
- ⁹ M. C. Daniel and D. Astruc, Gold nanoparticles: assembly, supramolecular chemistry, quantum-size-related properties, and applications toward biology, catalysis, and nanotechnology. *Chem Rev.* 2004, **104**, 293–346.
- ¹⁰ A. Desireddy, B. E. Conn, J. Guo, B. Yoon, R. N. Barnett, B. M. Monahan, K. Kirschbaum, W. P. Griffith, R. L. Whetten, U. Landman and T. P. Bigioni, Ultrastable silver nanoparticles. *Nature*, 2013, **501**, 399–402.
- ¹¹ E. Boisseliera and D. Astruc, Gold nanoparticles in nanomedicine: preparations, imaging, diagnostics, therapies and toxicity. *Chem. Soc. Rev.*, 2009, **38**, 1759–1782.
- ¹² N. G. Bastus, J. Comenge and V. Puntès, Kinetically Controlled Seeded Growth Synthesis of Citrate-Stabilized Gold Nanoparticles of up to 200 nm: Size Focusing versus Ostwald Ripening. *Langmuir* 2011, **27**, 11098–11105.
- ¹³ N. Li, P. Zhao and D. Astruc, Anisotropic Gold Nanoparticles: Synthesis, Properties, Applications, and Toxicity. *Angew. Chem. Int. Ed.*, 2014, **53**, 1756–1789.
- ¹⁴ A. M. Smith, M. C. Mancini and S. Nie, Bioimaging: second window for in vivo imaging. *Nat. Nanotechnol.*, 2009, **4**, 710–711.

- ¹⁵ J. Rodríguez-Fernández, J. Pérez-Juste, F. J. García de Abajo and L. M. Liz-Marzán, Seeded Growth of Submicron Au Colloids with Quadrupole Plasmon Resonance Modes. *Langmuir*, 2006, **22**, 7007–7010.
- ¹⁶ Y. Sun and Y. Xia, Increased Sensitivity of Surface Plasmon Resonance of Gold Nanoshells Compared to That of Gold Solid Colloids in Response to Environmental Changes. *Anal. Chem.*, 2002, **74**, 5297–5305.
- ¹⁷ C. M. Cobley, J. Chen, E. C. Cho, L. V. and Y. Xia, Gold nanostructures: a class of multifunctional materials for biomedical applications. *Chem. Soc. Rev.*, 2011, **40**, 44–56.
- ¹⁸ M. McEachran, D. Keogh, B. Pietrobon, N. Cathcart, I. Gourevich, N. Coombs and V. Kitaev, Ultrathin Gold Nanoframes through Surfactant-Free Templating of Faceted Pentagonal Silver Nanoparticles. *JACS*, 2011, **133**, 8066–8069.
- ¹⁹ B. Lim and Y. Xia, Metal Nanocrystals with Highly Branched Morphologies. *Angew. Chem. Int. Ed.*, 2011, **50**, 76–85.
- ²⁰ C. L. Nehl, H. Liao and J. H. Hafner, Optical properties of star-shaped gold nanoparticles. *Nano Lett.*, 2006, **6**, 683–688.
- ²¹ E. Ye, M. D. Regulacio, S.-Y. Zhang, X. J. Loh and M.-Y. Han, Anisotropically branched metal nanostructures. *Chem. Soc. Rev.*, 2015, **44**, 6001–6017
- ²² N. Cathcart and V. Kitaev, Multifaceted prismatic silver nanoparticles: synthesis by chloride-directed selective growth from thiolate-protected clusters and SERS properties. *Nanoscale*, 2012, **4**, 6981–6989.
- ²³ Y. Zhang, B. Wang, S. Yang, L. Li and L. Guo, Facile synthesis of spinous-like Au nanostructures for unique localized surface plasmon resonance and surface-enhanced Raman scattering *New J. Chem.*, 2015, **39**, 2551–2556.
- ²⁴ L. Pérez-Mayen, J. Oliva, A. Torres-Castro, E. De la Rosa. SERS substrates fabricated with star-like gold nanoparticles for zeptomole detection of analytes. *Nanoscale*, 2015, **7**, 10249–10258.
- ²⁵ W. Niu, Y. A. A. Chua, W. Zhang, H. Huang and X. Lu, Optical Properties of Star-Shaped Gold Nanoparticles *J. Am. Chem. Soc.*, 2015, **137**, 10460–10463.
- ²⁶ J. Aaron, E. de la Rosa, K. Travis, N. Harrison, J. Burt, M. José-Yacamán and K. Sokolov, Polarization microscopy with stellated gold nanoparticles for robust monitoring of molecular assemblies and single biomolecules. *Opt. Express*, 2008, **16**, 2153–2167.
- ²⁷ T. K. Sau and C. J. Murphy, Room temperature, high-yield synthesis of multiple shapes of gold nanoparticles in aqueous solution. *J. Am. Chem. Soc.*, 2004, **126**, 8648–8649.
- ²⁸ M. R. Langille, M. L. Personick, J. Zhang and C. A. Mirkin, Defining rules for the shape evolution of gold nanoparticles. *J. Am. Chem. Soc.*, 2012, **134**, 14542–14554.

- ²⁹ M. Yamamoto, Y. Kashiwagi, T. Sakata, H. Mori and M. Nakamoto, Synthesis and Morphology of Star-Shaped Gold Nanoplates Protected by Poly(N-vinyl-2-pyrrolidone). *Chem. Mater.*, 2005, **17**, 5391–5393.
- ³⁰ T. Huang, F. Meng and L. Qi, Controlled synthesis of dendritic gold nanostructures assisted by supramolecular complexes of surfactant with cyclodextrin. *Langmuir*, 2010, **26**, 7582–7589.
- ³¹ R. G. Weiner, C. J. DeSantis, M. B. Cardoso and S. E. Skrabalak, Diffusion and Seed Shape: Intertwined Parameters in the Synthesis of Branched Metal Nanostructures. *ACS Nano*, 2014, **8**, 8625–8635.
- ³² R. G. Weiner and S. E. Skrabalak, Metal Dendrimers: Synthesis of Hierarchically Stellated Nanocrystals by Sequential Seed-Directed Overgrowth. *Angew. Chem. Int. Ed.*, 2015, **54**, 1181–1184.
- ³³ R. G. Weiner, M. R. Kunz and S. E. Skrabalak, Seeding a New Kind of Garden: Synthesis of Architecturally Defined Multimetallic Nanostructures by Seed-Mediated Co-Reduction. *Acc. Chem. Res.*, 2015, **48**, 2688–2695.
- ³⁴ D. Schachter, The source of toxicity in CTAB and CTAB-stabilized gold nanorods. M.Sc Thesis, Rutgers 2013.
- ³⁵ H. Yuan, C. G. Khoury, H. Hwang, C. M. Wilson, G. A. Grant and T. Vo-Dinh, Gold nanostars: surfactant-free synthesis, 3D modelling, and two-photon photoluminescence imaging. *Nanotechnology*, 2012, **23**, 075102.
- ³⁶ R. de la Rica and M. M. Stevens, Plasmonic ELISA for the ultrasensitive detection of disease biomarkers with the naked eye. *Nat. Nanotechnol.*, 2012, **7**, 821–824.
- ³⁷ P. Gobbo, M. J. Biondi, J. J. Feld and M. S. Workentin, Arresting the time-dependent H₂O₂ mediated synthesis of gold nanoparticles for analytical detection and preparative chemistry. *J. Mater. Chem. B*, 2013, **1**, 4048–4051.
- ³⁸ D. Cecchin, R. de la Rica, R. E. S. Bain, M. W. Finnis, M. M. Stevens and G. Battaglia, Plasmonic ELISA for the detection of gp120 at ultralow concentrations with the naked eye. *Nanoscale*, 2014, **6**, 9559–9562.
- ³⁹ F. Yu, Z. Liu and W. Zhou, Facile Synthesis of (110)-Plane-Exposed Au Microflowers as High Sensitive Hydrogen Peroxide Sensors. *Eur. J. Inorg. Chem.* **2015**, 2528–2533.
- ⁴⁰ O. R. Bolduc and J.-F. Masson, Advances in Surface Plasmon Resonance Sensing with Nanoparticles and Thin Films: Nanomaterials, Surface Chemistry, and Hybrid Plasmonic Techniques. *Anal. Chem.*, 2011, **83**, 8057–8062.
- ⁴¹ S. Zeng, D. Baillargeat, H.-P. Hod, and K.-T. Yong, Nanomaterials enhanced surface plasmon resonance for biological and chemical sensing applications. *Chem. Soc. Rev.*, 2014, **43**, 3426–3452.

-
- ⁴² C. L. Cleveland, W. D. Luedtke, and U. Landman, Melting of Gold Clusters: Icosahedral Precursors. *Phys. Rev. Lett.*, 1998, **81**, 2036–2039.
- ⁴³ A. S. Barnard, A Thermodynamic Model for the Shape and Stability of Twinned Nanostructures. *J. Phys. Chem. B*, 2006, **110**, 24498–24504.
- ⁴⁴ M. A. Mahmoud, M. A. El-Sayed, J. Gao and U. Landman, High-Frequency Mechanical Stirring Initiates Anisotropic Growth of Seeds Requisite for Synthesis of Asymmetric Metallic Nanoparticles like Silver Nanorods. *Nano Lett.* 2013, **13**, 4739–4745.
- ⁴⁵ J. O'M. Bockris and L. F. Oldfield, The oxidation-reduction reactions of hydrogen peroxide at inert metal electrodes and mercury cathodes. *Trans. Faraday Soc.*, 1955, **51**, 249–259.
- ⁴⁶ B. R. Danger, D. Fan, J. P. Vivek and I. J. Burgess, Electrochemical Studies of Capping Agent Adsorption Provide Insight into the Formation of Anisotropic Gold Nanocrystals. *ACS Nano*, 2012, **6**, 11018–11026.
- ⁴⁷ N. Cathcart, A.J. Frank, V. Kitaev, Silver nanoparticles with planar twinned defects: effect of halides for precise tuning of plasmon resonance maxima from 400 to >900 nm. *Chem. Commun.*, 2009, **46**, 7170.
- ⁴⁸ Q. Zhang, N. Li, J. Goebel, Z. Lu and Y. Yin, A Systematic Study of the Synthesis of Silver Nanoplates: Is Citrate a “Magic” Reagent? *J. Am. Chem. Soc.*, 2011, **133**, 18931–18939.
- ⁴⁹ G. S. Métraux and C. A. Mirkin, Rapid Thermal Synthesis of Silver Nanoprisms with Chemically Tailorable Thickness. *Adv Mater.*, 2005, **17**, 412–415.
- ⁵⁰ R. Jin, Y. Cao, E. Hao, G. S. Métraux, G. C. Schatz, C. A. Mirkin, Controlling anisotropic nanoparticle growth through plasmon excitation. *Nature*, 2003, **425**, 487–490.
- ⁵¹ J. E. Millstone, W. Wei, M. R. Jones, H. Yoo and C. A. Mirkin, Iodide Ions Control Seed-Mediated Growth of Anisotropic Gold Nanoparticles. *Nano Lett.*, 2008, **8**, 2526–2529.
- ⁵² J. Kimling, M. Maier, B. Okenve, V. Kotaidis, H. Ballot and A. Plech, Turkevich Method for Gold Nanoparticle Synthesis Revisited. *J. Phys. Chem. B*, 2006, **110**, 15700–15707.
- ⁵³ K. D. Hartlen, A. P. T. Athanopoulos and V. Kitaev, Facile Preparation of Highly Monodisperse Small Silica Spheres (15 to >200 nm) Suitable for Colloidal Templating and Formation of Ordered Arrays. *Langmuir* 2008, **24**, 1714–1720.
- ⁵⁴ L. B. Wright, N. A. Merrill, M. R. Knecht and T. R. Walsh, Structure of Arginine Overlayers at the Aqueous Gold Interface: Implications for Nanoparticle Assembly. *ACS Appl. Mater. Interfaces*, 2014, **6**, 10524–10533.
- ⁵⁵ G. Plascencia-Villa, D. Torrente, M. Marucho, M. Joseř-Yacamaě, Biodirected Synthesis and Nanostructural Characterization of Anisotropic Gold Nanoparticles. *Langmuir*, 2015, **31**, 3527–3536.

⁵⁶ Z. Quan, Y. Wang and J. Fang, High-Index Faceted Noble Metal Nanocrystals. *Acc. Chem. Res.*, 2013, **46**, 191 –202.